Repairing native defects on EUV mask blanks

Mark Lawliss[a], Emily Gallagher[a], Michael Hibbs[a] , Kazunori Seki[b], Takeshi Isogawa[b], Tod Robinson[c] , Jeff LeClaire[c]
[a]IBM Microelectronics Div., 1000 River Street, Essex Junction, VT 05452;
[b]Toppan Photomasks Inc., 1000 River Street, Essex Junction, VT 05452;
[c]RAVE LLC, 430 S. Congress Avenue, Suite 7, Delray Beach, FL, 33445, USA

ABSTRACT

Mask defectivity is a serious problem for all lithographic masks, but especially for EUV masks. Defects in the EUV blank are particularly challenging because their elimination is beyond control of the mask fab. If defects have been identified on a mask blank, patterns can be shifted to place as many blank defects as possible in regions where printing impact will be eliminated or become unimportant. For those defects that cannot be mitigated through pattern shift, repair strategies must be developed. Repairing defects that occur naturally in the EUV blank is challenging because the printability of these defects varies widely. This paper describes some types of native defects commonly found and begins to outline a triage strategy for defects that are identified on the blank. Sample defects best suited to nanomachining repair are treated in detail: repairs are attempted, characterized using mask metrology and then tested for printability. Based on the initial results, the viability of repairing EUV blank native defects is discussed.

Keywords: EUV, mask defect repair, defect printability, nanomachining

1. INTRODUCTION

Mask customers require wafer patterning results that are not impacted by printing defects, even during early development cycles. Historically, the majority of defects encountered at DUV mask inspection are generated during the mask fabrication process, since the associated optical mask blanks are nearly defect free. The situation for incoming EUV blanks is different since the vast majority are not defect free at this stage of development.[1] These incoming blank defects must be considered when determining a mask fabrication strategy. One strategy is to shift the entire mask pattern at the initial print step, within pattern centrality limits, to ensure that if not all, then at least, the most impactful blank defects avoid critical design areas.[2] This is shown in Figure 1.

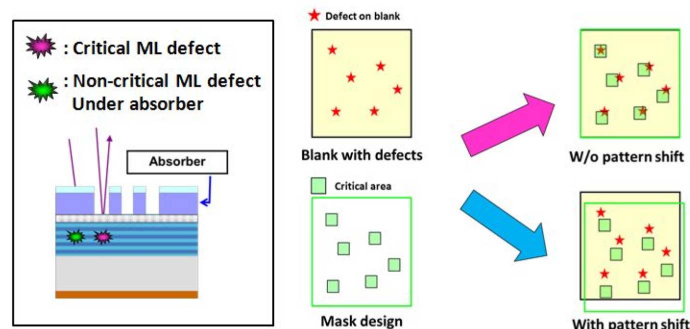

Figure 1. The technique of pattern shift to avoid critical defects is shown in this schematic. The cross-sectional view of the final mask is shown on the left. A critical defect is shown below the clear area where print errors could be maximized, while the defect covered by the absorber area is considered non-critical. The mask top-down views in the center highlight the defects on the blank and the areas of interest on the mask design. On the right, the combination of pattern layout and blank defects is shown both without pattern shift and with an effective pattern shift.

It is important to consider that current inspection capability is not actinic for EUV blanks. Consequently, defect detection and characterization may not be perfect. Therefore, even if pattern shift is effective, there may be unexpected blank

Photomask Technology 2014, edited by Paul W. Ackmann, Naoya Hayashi, Proc. of SPIE
Vol. 9235, 923516 · © 2014 SPIE · CCC code: 0277-786X/14/$18 · doi: 10.1117/12.2069787

Downloaded From: http://proceedings.spiedigitallibrary.org/ on 11/25/2014 Terms of Use: http://spiedl.org/terms

defects landing in critical patterned regions, so some blank defect repair capability may be required. Conventional repair methods may be used and adapted to address non-standard defects.

In this paper, we developed initial repair strategies for blank defects that would result in wafer printing errors if not improved. In Section 2, we describe a method for fabricating an EUV mask with known blank defects for repair consideration. Characterization of a range of blank defects using multiple techniques is provided. These techniques included defect images obtained from scanning electron microscope (SEM), defect mapping by an atomic force microscope (AFM) and wafer print results obtained before any mitigation. In Section 3, we describe a new repair strategy using an established nanomachining method. Pre-repair wafer simulation is considered as an option to provide repair parameters. Details of post-repair results are provided and compared in Section 4. Finally, the results obtained are used to propose future work in mask blank repair.

2. DEFECT MASK FABRICATION AND CHARATERIZATION

2.1 Method for creating a blank defect mask

The EUV blank used for this work was built with the standard films: 2.5nm of Ru-capping layer, 40 pairs of Mo/Si bi-layers on the substrate and backside film of CrN. The method for fabricating a mask placing patterns over targeted blank defects has been described in previous work. [3],[4] The first step was to a add a set of alignment marks with a lithographic process. These marks are used to define positional accuracy of future inspections and to locate and define areas of defects in the original blank. After the alignment marks are added, 193nm blank inspections were completed. Defect detections were evaluated and sites were selected that met a criteria based on the likelihood the site would cause a print error on the final mask if located in a critical pattern area. The next step was to deposit the standard Ta-based absorber. A key characteristic to highlight is that any defect that resulted in a print error on the final mask at one of these previous locations would be clearly traced to a blank defect and not an absorber defect formed during the normal mask processing. To increase the chance our key blank defects would land in a key pattern area, and not under absorber film, we used a "reverse defect avoidance" technique. A print tool job deck was created to align a 5x5 array of 1:1 pitch 160nm contact features over each defect of interest. Our goal for this work was to understand print defects in relaxed pattern sizes, not to demonstrate at the smallest features available. The selected patterns provide a good learning vehicle for repair strategies and methods. The process flow used is described in Figure 2 below.

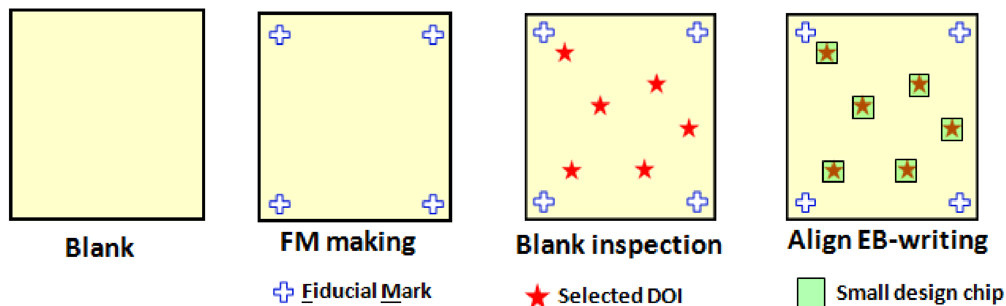

Figure 2. A process flow for creating a blank defect test mask is shown. It includes adding fiducial marks, performing a blank inspection and added small pattern "chips" at selected defects of interest.

2.2 Blank defect mask characterization

After the EUV blank test mask was created, the next step was to characterize the mask. This characterization included obtaining SEM defect images, defect mapping from an atomic force microscope (AFM) and obtaining wafer print

Downloaded From: http://proceedings.spiedigitallibrary.org/ on 11/25/2014 Terms of Use: http://spiedl.org/terms

results. In our previous work, one goal was to characterize blank inspection tool results. [3] In this work, while we relied on inspection to detect defective areas, the main focus was to select the sites that provided opportunity for repair. The defects selected for repair work were small enough to be contained within one mask feature, were visible when mapped by AFM, and caused a measurable print error. If a characterized defect was very large, and impacted several features, it was excluded from this work. The assumption is that these large defects should be eliminated by the blank supplier or avoided during pattern write. If the wafer printing error was very subtle, it was also not considered so that ambiguous results could be avoided. For the 160nm sized contacts in this work, even small defects contained within a contact feature cause significant errors on the wafer and the process window for successful repairs is small. For photomasks in general, contact feature repair requires the most robust process. This work demonstrates that EUV masks are consistent.

After mask characterization, several defects were selected suitable to include in this work. In almost every case, the defect found at blank inspection was well-centered in a 5x5 array of contacts. In Figure 3 below, the set of defects used for repair testing is shown. In each case, the defect is easily mapped with one contact feature and the wafer print has significant error.

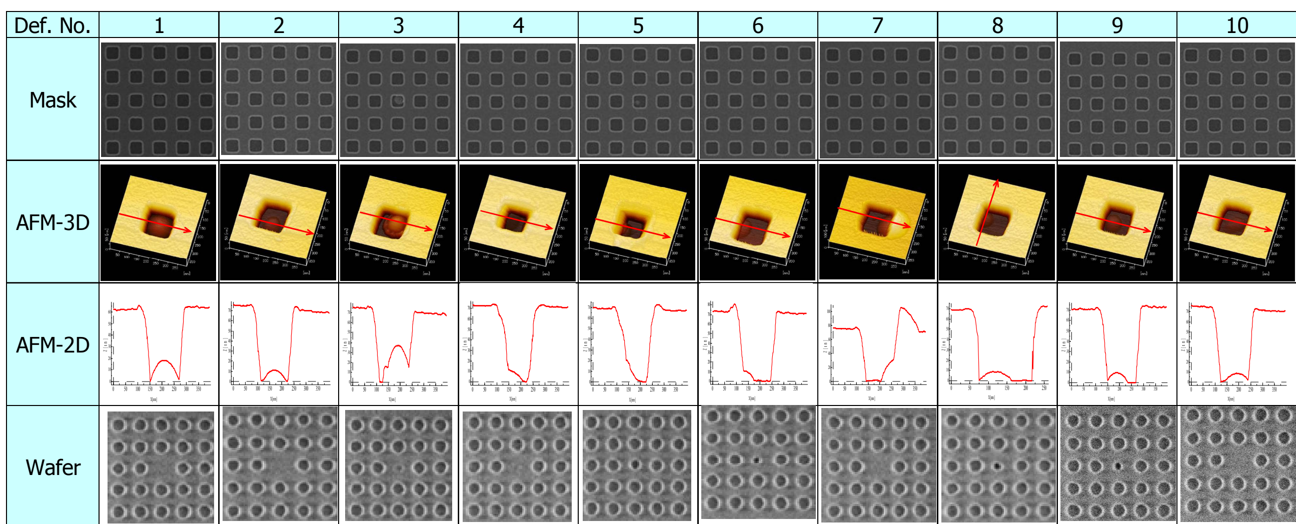

Figure 3. Ten blank defects used for repair testing are shown. All were contained within one feature and are clearly visible in the AFM images in rows 2 and 3. Row 4 shows Pre-Repair wafer prints. Some of the defects print as a completely missing contact on wafer, while some print as a reduced contact size on wafer.

3. REPAIR STRATEGIES AND SIMULATIONS

It is expected that some repair will be required to fabricate EUV masks that are defect free for printing. The standard repair strategies include processes for absorber repair and removal of foreign particles on the surface. A blank defect repair process will be required for EUV masks, even if progress is made on defect reduction during the blank manufacturing process and some defects are avoided by a pattern shifting routine at the mask write. New repair strategies using existing repair tool platforms will be required for these blank defects. We will use some of the defects identified in the previous section to develop these new strategies.

The defects that will be repaired as part of this work were identified by blank inspection before the absorber was deposited. It is likely there will be removal of material of unknown composition, depending on where in the multilayer deposition process the defect was added. In some cases, the defect will be under the multilayers on or in the substrate. In other cases the defect may be buried in the stack. Clearly, the depth extent of the defect in these cases is below the capping layer and potentially compromising reflectivity, rendering standard repair inappropriate. Standard defect repair for defects with a measurable height above the mask surface usually involve a subtle depth bias and small amount of

Downloaded From: http://proceedings.spiedigitallibrary.org/ on 11/25/2014 Terms of Use: http://spiedl.org/terms

edge absorber bias to achieve good printability. This strategy may leave an insufficient reflectivity at a blank defect site if some of the foreign material remains embedded. For these defects, one theory suggests a more aggressive strategy with larger depth bias and larger lateral edge absorber bias. We call this method repair process #A. This process will involve a depth removal that will be even across the whole contact feature area. The increased depth bias may be effective in removing the embedded particle, while the lateral absorber bias will compensate for the reduced number of multilayers. Figure 4 below shows a schematic of a blank defect and the two repair strategies described above, with the repair process #A on the right. In all schematics, the purple shape indicates the defect area, but does not indicate defect composition nor defect mechanism.

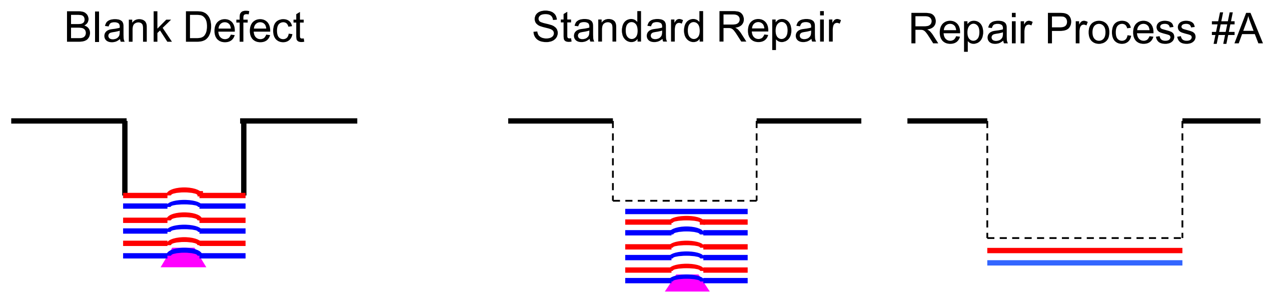

Figure 4. Shown above are schematics of a blank defect on the left, the standard particle removal repair technique in the middle and a more aggressive repair strategy on the right. The more aggressive repair includes a depth bias removing multilayer pairs and absorber bias.

A second alternate strategy, repair process #B, will also be considered as part of this work. The targeted repair strategy will also remove multilayer material, but only in the immediate region of the defect area. Some edge absorber lateral bias may also be needed to achieve good printability. This method is shown in the schematic in Figure 5.

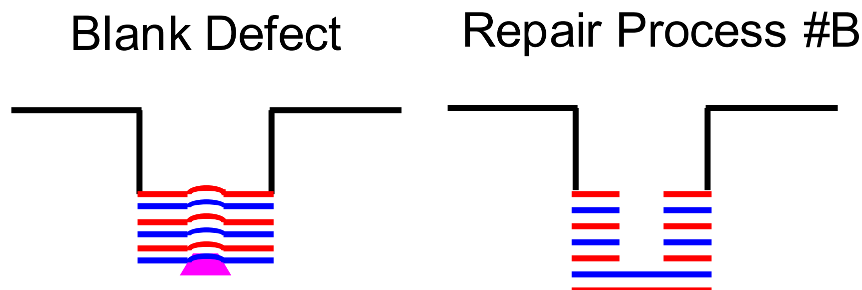

Figure 5. Shown above are schematics of a blank defect on the left, the a targeted repair strategy on the right in which multilayer are missing from the structure.

In production, the proper repair targets for each individual defect may be obtained from pre-repair defect simulation of each site. To help understand the benefit of this type of simulation, some defects on this mask were mapped and input to a wafer print simulation program. Input into the program included mask film composition and film heights, defect size based on AFM mapping and potential repair strategies. A production level repair will require feature CD to match target through a prescribed focus range. One of the benefits of this simulation work is to understand the repair parameters predicted to meet this printing requirement. The challenge is to balance the computing time versus a reasonable range of possible input parameters. In our case, the focus was on repair strategy #B. This strategy was used on line and space

Downloaded From: http://proceedings.spiedigitallibrary.org/ on 11/25/2014 Terms of Use: http://spiedl.org/terms

patterns in some previous work and resulted in Bossung curves that were flat through the process window of interest on these line and space simulations. [5] In Figure 6, the schematic shows both the simulated cross-section and the resultant aerial image for three cases. The bottom row illustrates one possible repair strategy and the improved aerial image.
.

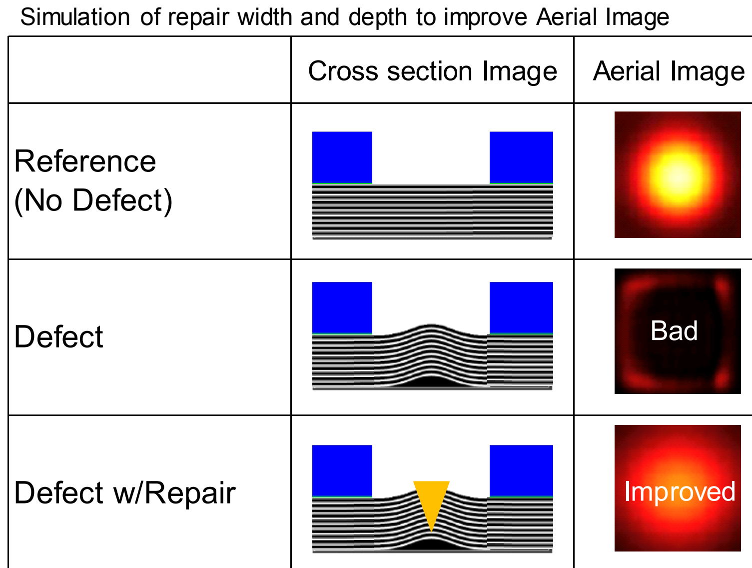

Figure 6. Shown above are the 2D EUV mask stack input to the simulator and the associated aerial image created by EUV illumination. The top row is a reference space without any defect, the middle row introduces a defect and the bottom row shows one possible repair shape in yellow and the improved aerial image. Simulation can be sued to explore repair parameters and recommend ones for repair on the mask that will improve the wafer aerial image.

All repair work described here was accomplished using a nanomachine repair method. This method has a known strength of removing material of unknown composition to aggressive targets. Both the depth and lateral edge absorber bias repair tolerances were set to <3nm for all sites. The resulting repairs achieved these tolerances, with the range of depths 0nm to 58nm, and the edge absorber bias 0nm to 58nm. The range of repair bias in this work was an initial choice, but larger biases may ultimately required. The repair parameters for repair process #B, including the 70nm depth target, were provided by wafer simulation. None of the repairs, including repair process #B, required the high aspect ratio nanobit to meet the +/- 3nm tolerance. The majority of the process debris created by the repairs was removed with the BitClean process available on the same system used to do the repairs. Figure 7 below shows the scan image results on four sites. The contact on the left scan used repair process #B removing multilayer in the area around the original defect area, while the contacts in the other scans used repair process #A removing multilayers across the whole contact. The print results shown in Section 4 were not constrained by repair process control.

Downloaded From: http://proceedings.spiedigitallibrary.org/ on 11/25/2014 Terms of Use: http://spiedl.org/terms

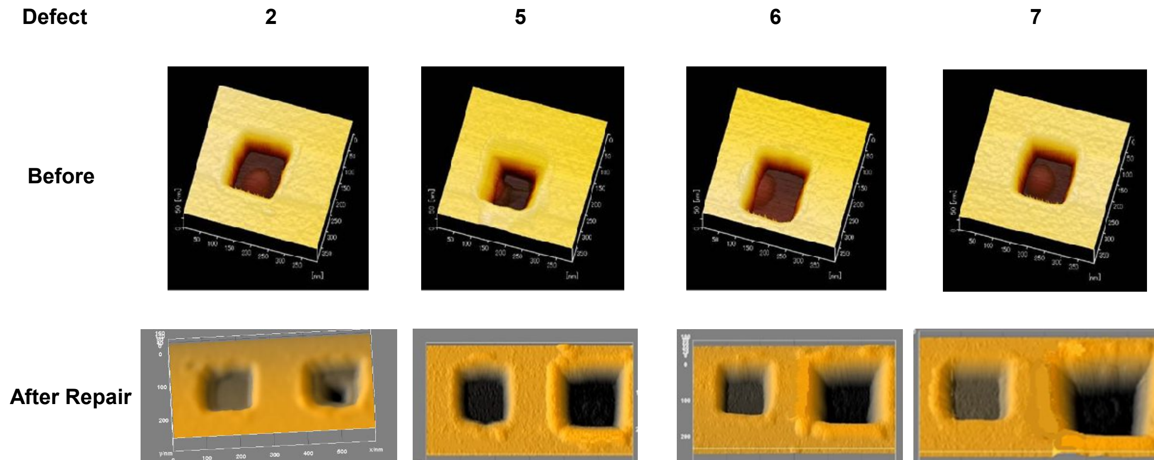

Figure 7. The scans show four repairs, the initial defect is on the top row and a pair is provided after repair so that a reference (left) and the repaired site (right) can be compared. Only the contact on the far left was repaired using test process #B in which a targeted depth of 70nm was achieved with nanomachine repair. The other three sites were repaired using repair process #A. Both the contact size and depth are increased with nanomachine repair. Please note that some scans show ghost artifacts from the software and AFM scan methods used.

4. REPAIR RESULTS AND PRINTABILITY

After mask repair and cleaning, the repair results must be assessed though printability. There were ten repair sites completed for print review. For each of the ten sites, the wafer CD of the defective contact before repair was drastically reduced from target. For five of the sites, the contact was completely missing before repair. To assess the sites after repair, the mask was measured using an EUV microscope.[6] The illumination used was quasar NA=0.33, consistent with realistic contact exposure conditions on an EUV scanner.

A graphical representation of the data is shown in Figure 8. The red bar represents the pre-repair CD size as a percentage of reference target. The blue bar is the same measurement after repair. The desired result is for the blue bar to reach 100%. The first important result is site 1, which used the standard repair process with very small bias in depth and little absorber edge bias. For this site, the site printed a missing contact both before and after repair, indicating that standard methods will not be effective on blanks defects. Every other site shows improvement after repair. A few of the sites approached the 100% CD print target.

The other site of note is defect #2. This site was repaired using the repair process #B strategy based on wafer simulation software input. Repair process #B was a targeted depth bias covering only the area of the original defect rather than the whole contact. While the print CD size did improve, the amount of improvement was less than achieved on all repair process #1 sites. The most obvious next step on this site is to increase the lateral edge absorber bias beyond the amount indicated by the simulation. So far, repair process #A is more effective in improving printability. As previously discussed, contact repair is challenging, but these results suggest a path forward.

Downloaded From: http://proceedings.spiedigitallibrary.org/ on 11/25/2014 Terms of Use: http://spiedl.org/terms

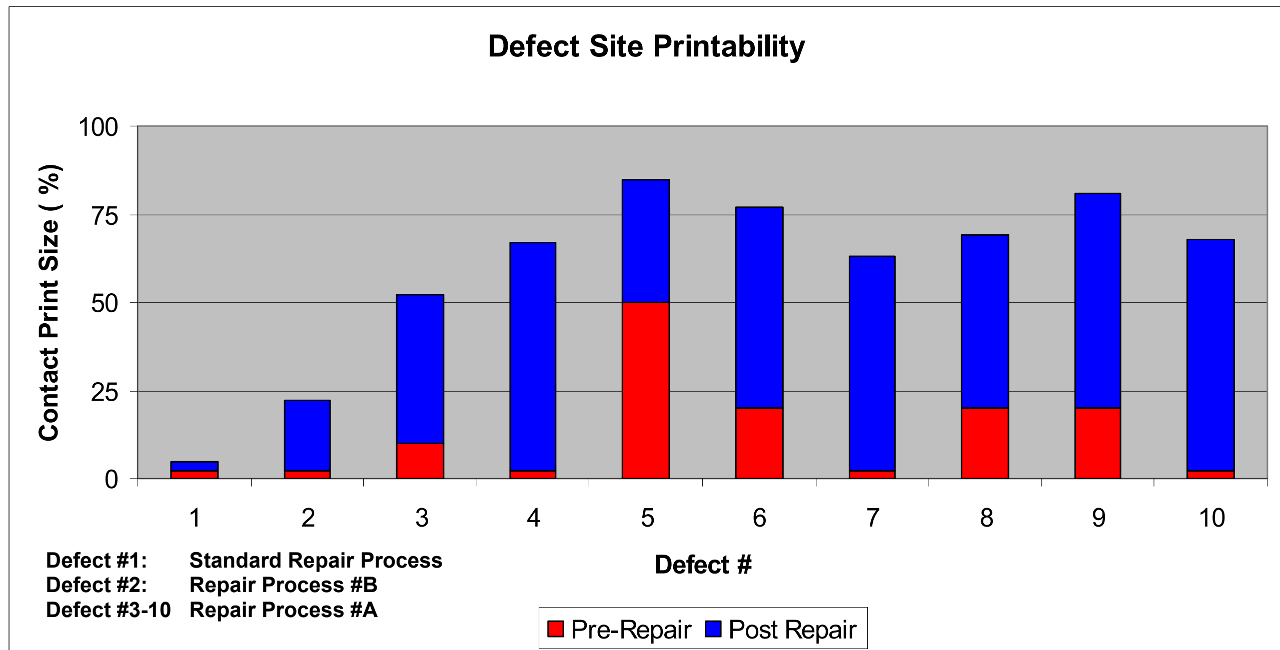

Figure 8. This bar chart shows the pre-repair and post-repair contact print size by percentage for the ten sites measured. Each site showed printability improvement, except for site 1, which used the standard repair method.

Figure 9 plots the same data. In this chart, each site is analyzed for CD error % improvement after repair, and is graphed against both depth bias and XY edge absorber bias. This graph shows a trend of greater CD error % improvement with higher repair bias. The XY edge absorber bias shows a much stronger trend.

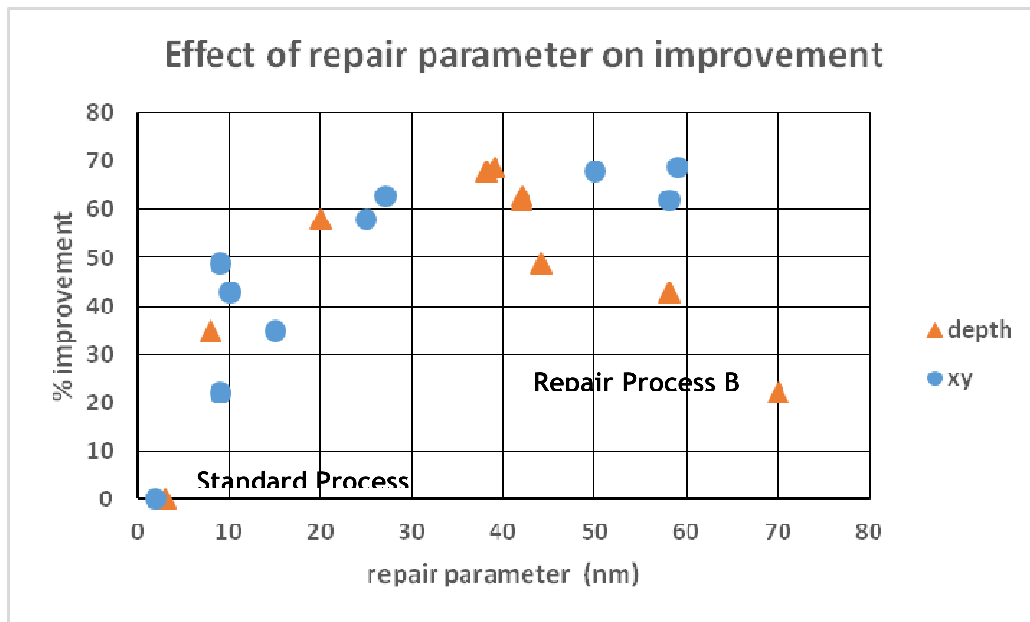

Figure 9. This graph plots the post repair print improvement (% improvement) versus both depth bias (nm) and lateral edge absorber bias (nm). Both parameters show a positive trend with the absorber bias trend stronger.

Downloaded From: http://proceedings.spiedigitallibrary.org/ on 11/25/2014 Terms of Use: http://spiedl.org/terms

The repair site that gave the best final printability image was defect #5. This site was repaired using repair process #A. Figure #10 contains some images of the site, both before and after repair.

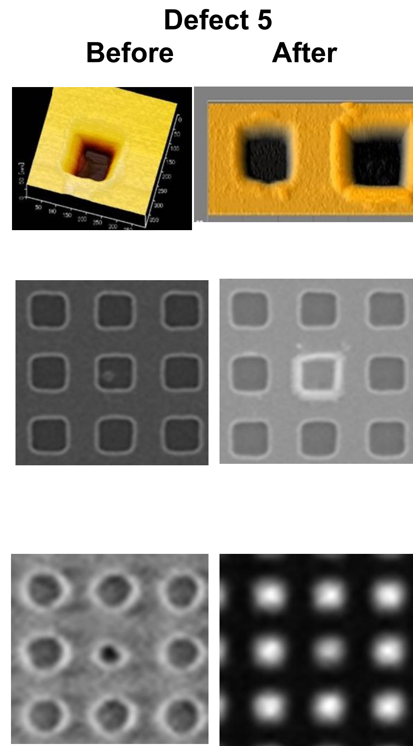

Figure 10. The images show defect #5 both before and after repair. The top row shows the AFM image of the site. The center row shows the SEM image of the site. The bottom row shows a wafer print of the site before repair and an EUV microscope image of the site after repair. The printability of this site has improved by almost 30%.

5. SUMMARY

A method for fabricating a blank defect test mask was described. This fabrication involved placing a small array of critical features over each of a set of blank defects to allow for characterization and repair. The method for characterizing these defects was detailed. It was discovered that blank defects can cause a full range of print effects, from subtle all the way to catastrophic. This new test mask had a sufficient number of repair site candidates and a number of repairs were performed. The nanomachining technique was effective in executing the repairs as prescribed. While the final print results were not perfect, trends were discovered that could determine our next steps. The strongest trend is that increased lateral edge absorber bias could improve printability even further. The repair sites described in this work are still available for further improvement to prove these trends. The next proposed development will focus on determining the repair parameters with each method that will result in contact printability approaching 100% with sufficient process window. We will also develop the proper methods to utilize pre-repair simulation to provide these repair parameters.

Downloaded From: http://proceedings.spiedigitallibrary.org/ on 11/25/2014 Terms of Use: http://spiedl.org/terms

ACKNOWLEDGEMENTS

The authors would like to thank the following groups for their contributions to this paper: the SEMATECH/LBNL SHARP* team for microscope images, IBM manufacturing teams in Burlington and Albany for mask processing and the IBM EUV team in Albany for wafer simulation support. Finally we would like to thank the IBM Toppan and RAVE management and technical teams for support of this project.

*SHARP work was performed under the auspices of the U.S. Department of Energy by the University of California Lawrence Berkeley National Laboratory under management and operating contract DE-AC02-05CH11231.

REFERENCES

[1] Antohe, Alin O., et al. "Production of EUV mask blanks with low killer defects." Proc. SPIE 9048 (2014).

[2] Negishi, Y., et al, "Using pattern shift to avoid blank defects during EUVL mask fabrication," Proc. SPIE 8701 (2013).

[3] Gallagher, E., et al, "Learning from native defects on EUV mask blanks," Proc. SPIE 9256 (2014).

[4] Gallagher, E., et al, "EUVL mask repair: expanding options with nanomachining," Proc. SPIE 8522 (2012).

[5] McIntyre, G., et al, "Through-Focus EUV multilayer defect repair with nanomachining" Proc. SPIE 8679 (2013).

[6] Kenneth A. Goldberg et al., "The SEMATECH high-NA actinic reticle review project (SHARP) EUV mask-imaging microscope," Proc. SPIE 8880 (2013).

Downloaded From: http://proceedings.spiedigitallibrary.org/ on 11/25/2014 Terms of Use: http://spiedl.org/terms